



Landslide mapping with deep learning: the role of pre-/post-event SAR features and multi-sensor data fusion

Aiym Orynbaikyzy, Frauke Albrecht, Wei Yao, Mahdi Motagh, Wandi Wang, Sandro Martinis & Simon Plank

To cite this article: Aiym Orynbaikyzy, Frauke Albrecht, Wei Yao, Mahdi Motagh, Wandi Wang, Sandro Martinis & Simon Plank (2025) Landslide mapping with deep learning: the role of pre-/post-event SAR features and multi-sensor data fusion, GIScience & Remote Sensing, 62:1, 2502214, DOI: [10.1080/15481603.2025.2502214](https://doi.org/10.1080/15481603.2025.2502214)

To link to this article: <https://doi.org/10.1080/15481603.2025.2502214>



© 2025 The Author(s). Published by Informa UK Limited, trading as Taylor & Francis Group.



[View supplementary material](#)



Published online: 13 May 2025.



[Submit your article to this journal](#)



Article views: 1541




[View related articles](#)



[View Crossmark data](#)

Landslide mapping with deep learning: the role of pre-/post-event SAR features and multi-sensor data fusion

Aiym Orynbaikyzy^a, Frauke Albrecht^{b,c}, Wei Yao^d, Mahdi Motagh^{e,f}, Wandi Wang^{e,f}, Sandro Martinis^a and Simon Plank^g 

^aGerman Remote Sensing Data Center (DFD), German Aerospace Center (DLR), Oberpfaffenhofen, Wessling, Germany; ^bHelmholtz Artificial Intelligence Cooperation Unit, German Climate Computing Center (DKRZ), Hamburg, Germany; ^cHelmholtz-Zentrum Hereon, Geesthacht, Germany; ^dRemote Sensing Technology Institute (IMF), German Aerospace Center (DLR), Oberpfaffenhofen, Wessling, Germany; ^eSection of Remote Sensing and Geoinformatics, GFZ Helmholtz Centre for Geosciences, Potsdam, Germany; ^fInstitute of Photogrammetry and Geoinformation, Leibniz University Hannover, Hannover, Germany

ABSTRACT

Landslide mapping is critically important for providing detailed spatial information on hazard extent in a timely manner that ultimately contributes to the protection of human lives and critical infrastructure. In the context of increasing demands for scalable and automated solutions, Earth Observation (EO) data coupled with deep learning offer great potential to enhance the speed and accuracy of emergency mapping. This study explores the utility of a deep learning model with the U-Net architecture for automated landslide mapping using data from optical Sentinel-2 and Synthetic Aperture Radar (SAR) Sentinel-1 satellites. We investigate the effectiveness of various optical (visible, near-infrared, and short-wave infrared) and SAR-derived features (backscatter coefficients, polarimetric features, interferometric coherence), used both independently and in combination. Additionally, we assess the impact of increasing the number of pre-/post-event SAR observations on classification performance. The U-Net models are trained and tested using globally distributed and limited reference data (563 unique patches). Optical features consisted of one pre-/post-event feature, whereas SAR features had three for each reference sample. Our analysis shows that the highest classification accuracies are consistently achieved using optical features (F1-score of 0.83 with visible, near-, and short-wave infrared bands). No substantial improvements were recorded when SAR features were combined with optical features. The usage of the most common optical features (visible and near-infrared) shows the lowest accuracies compared to their combination of short-wave infrared or red-edge bands. Increasing the number of pre-/post-event SAR features improves the SAR-based accuracies. To promote further advancements in automated landslide mapping using deep learning, the landslide reference dataset generated in this study is freely available at (<https://doi.org/10.5281/zenodo.15284357>).

ARTICLE HISTORY

Received 25 October 2024
Accepted 24 April 2025

KEYWORDS

Landslide classification;
optical data; SAR data; deep
learning

1. Introduction


Landslides, as a significant natural hazard, pose a substantial threat to human lives, infrastructure, and the environment. The projected increase in extreme weather events and ongoing rapid informal urbanization are anticipated to amplify the frequency and severity of landslide hazards worldwide (Froude and Petley 2018; Ozturk et al. 2022). Despite significant scientific efforts to predict the timing and location of landslides (Guzzetti et al. 2020), they often occur unexpectedly (van Westen Cj et al. 2006). Therefore, accurate and comprehensive landslide mapping is of vital importance for effective disaster management and risk reduction.

Landslide mapping has gone through significant advancements with the usage of Earth Observation

(EO) datasets, which became one of the primary sources for monitoring landslide processes (Guzzetti et al. 2012). Recent developments in machine learning (ML) and deep learning (DL) solutions have further propelled the field (Zhong et al. 2020). DL, in particular, offers several advantages over the traditional ML or statistical methods, particularly when dealing with large EO datasets. As outlined by Tehrani et al. (2022), DL excels at capturing non-linear relationships with multi-dimensional remote sensing data and autonomously learns complex spatial and temporal patterns present in the data. This substantially reduces or eliminates the labor-intensive feature engineering tasks, which typically require domain-specific expertise. Recent comparative studies on the performance of conventional machine learning

CONTACT Aiym Orynbaikyzy  aiym.orynbaikyzy@dlr.de

This article has been corrected with minor changes. These changes do not impact the academic content of the article.

 Supplemental data for this article can be accessed online at <https://doi.org/10.1080/15481603.2025.2502214>

© 2025 The Author(s). Published by Informa UK Limited, trading as Taylor & Francis Group.

This is an Open Access article distributed under the terms of the Creative Commons Attribution-NonCommercial License (<http://creativecommons.org/licenses/by-nc/4.0/>), which permits unrestricted non-commercial use, distribution, and reproduction in any medium, provided the original work is properly cited. The terms on which this article has been published allow the posting of the Accepted Manuscript in a repository by the author(s) or with their consent.

classifiers (e.g. Random Forest and Support Vector Machine) and state-of-the-art DL models showed the superior performance of the last (Ghorbanzadeh et al. 2019; Prakash, Manconi, and Loew 2020; Wang et al. 2021). In the context of landslide mapping using EO data and DL, the primary objective is typically to generate a binary layer that distinguishes landslide-affected pixels from non-landslide pixels. This task falls under the category of semantic segmentation, wherein each pixel in an image is assigned a specific class label. A vast number of semantic segmentation models have been applied and compared for their landslide mapping capabilities, ranging from classical convolutional architectures like U-Net (Ronneberger, Fischer, and Brox 2015) to more advanced frameworks such as DeepLabv3+ (Chen et al. 2018) and HRNet (Wang et al. 2019). While models like U-Net are favored for their simplicity and effectiveness on small datasets, more sophisticated approaches, such as DeepLabv3+ and HRNet, demonstrate superior performance in handling complex landscapes and boundary delineations due to their ability to capture multiscale features and maintain high-resolution representations (Jin, Liu, and Huang 2024; Yang et al. 2022). However, these advanced models come with increased computational demands. Additionally, transformer-based models such as SegFormer are now gaining popularity for remote sensing applications, offering state-of-the-art accuracy, though they require larger training datasets to perform optimally (Ghorbanzadeh, Xu, Zhao, et al. 2022). Given the limited training data available for this study, we selected U-Net for this study due to its proven effectiveness on small datasets and its widespread adoption in the geoscientific community, aligning with our data-driven research objectives (Ganerød et al. 2023; Nava et al. 2022; Li et al. 2022).

A persistent challenge in landslide mapping, especially when applying advanced ML/DL techniques, is the limited availability of high-quality reference data. Some studies have attempted to address this issue using contrastive self-supervised learning (Ghorbanzadeh et al. 2024) or data augmentation strategies (Soares et al. 2020; Woodard et al. 2023), but these methods often rely on expansive global datasets or sophisticated algorithms to compensate for data scarcity. Publicly available benchmark datasets (Ghorbanzadeh, Xu, Ghamisi, et al. 2022; Meena et al. 2023; Xu et al. 2024) offer large volumes of data for comparing ML models; however, they frequently lack crucial landslide-specific metadata, such as georeferenced footprints and precise occurrence dates. This absence makes it difficult to address more complex geo-environmental research questions, such as analyzing the influence of specific environmental factors.

Apart from data scarcity, choosing the right input features is critical for model accuracy. In recent years, the combination of optical and SAR features has become one of the prominent topics in remote sensing research due to the complementary characteristics of these datasets. The launch of high-resolution Sentinel-1 and Sentinel-2 satellites has enabled numerous studies to explore the benefits of integrating both sensor types for various applications, including land use and land cover classification (Joshi et al. 2016), crop type mapping (Orynbaikyzy, Gessner, and Conrad 2019), flood detection (Fichtner et al. 2023), and landslide detection (Fu et al. 2024). However, in the context of natural hazards, particularly landslides, the advantages remain inconclusive (Mondini et al. 2021). Unlike agricultural studies, which benefit from multi-temporal data across growing seasons (Orynbaikyzy et al. 2020), landslide mapping requires near-real-time outputs for emergency response. Rainfall-triggered landslides often occur under adverse weather, making optical data unavailable when needed most. In such cases, SAR imagery is essential due to its all-weather capabilities. However, SAR data is prone to geometric distortions in mountainous regions and increased noise in vegetated areas, which can reduce detection accuracy (Lindsay et al. 2023). While optical-SAR fusion shows promise, its effectiveness is application-specific and still under-researched for landslide mapping, particularly in time-critical scenarios (Lacroix, Handwerker, and Bièvre 2020; Sivasankar, Ghosh, and Joshi 2021; Nava et al. 2022). To maximize the benefits of optical-SAR fusion, understanding the contributions of individual features is essential. Many landslide studies rely on very high-resolution (VHR) EO data to capture changes in terrain morphology, surface characteristics, and vegetation cover. Since most VHR optical sensors primarily include visible and near-infrared (NIR) bands, these features are the most common choice for landslide mapping (Soares et al. 2022; Yang and Xu 2022). The spectral shifts indicative of modified surface properties resulting from ground movements contribute to the identification of areas impacted by landslides. Additionally, the red-edge (RE) and short-wave infrared (SWIR) bands offer valuable insights into vegetation health and moisture content, expanding beyond the capabilities of visible and NIR bands (Lu et al. 2021). However, the application of these bands (RE, SWIR) in landslide mapping using deep learning methods remains underexplored.

Although SAR data is less frequently used than optical data, key features such as interferometric coherence and amplitude are widely employed to detect surface deformation associated with landslides (Jelének and Kopačková-Strnadová 2021; Nava,

Monserat, and Catani 2022; Zhang et al. 2022). Interferometric coherence measures the degree of similarity in phase between two SAR images, capturing changes in surface deformation, while amplitude represents the strength of the reflected radar signal, revealing variations in surface characteristics caused by landslide activity. However, despite the advancements, the application of SAR features in DL for landslide mapping remains underexplored. Recent findings suggest (Nava et al. 2022) that incorporating multiple pre- and post-event SAR scenes can significantly improve model performance by capturing temporal dynamics and enhancing the detection of subtle surface changes. Furthermore, SAR polarimetry, which analyses radar wave polarization states, could provide additional insights into a more comprehensive understanding of landslide dynamics (Plank, Twele, and Martinis 2016) but has been insufficiently studied in this context.

Despite the increasing number of studies dedicated to employing deep learning techniques in landslide mapping, certain research questions remain underexplored. Here, we address the following research questions:

- Does the integration of optical and SAR features result in higher classification accuracies compared to their individual usage?
- Does the increase in the number of pre- or post-event Sentinel-1 scenes contribute to enhancing the U-Net performance?
- Would the usage of additional spectral bands (e.g. SWIR and RE) or SAR polarimetric features compared to a conventional set of features help to increase the classification accuracies?

This study aims to contribute to above listed open issues by evaluating the landslide classification performance of the commonly used semantic segmentation model, U-Net, using a wide variety of optical features from Sentinel-2 and SAR features from Sentinel-1 derived based on the limited but globally distributed reference data.

2. Study sites and data

2.1. Landslides inventory

The supervised machine learning requires labeled reference data for building the model. Depending on the properties of the selected classifier, requirements for training data may differ (Foody et al. 2006). For deep learning classification models such as U-Net, the

quality and quantity of the training data have a significant impact on model performance. While a large sample size allows the model to learn more complex relationships present in the data, the samples' quality ensures the accuracy and reliability of the model.

To address our research objectives, we decided to compile a landslide inventory based on reported large landslides that occurred worldwide from July 2015 onwards (Figure 1). The temporal threshold was chosen to acquire both, Sentinel-1 and Sentinel-2 data, for the same landslide event. Apart from landslides in southern Kyrgyzstan, the great majority of the landslides were first discovered based on a report on The Landslide Blog¹ and then visually interpreted using the pre- and post-event Sentinel-2 and Sentinel-1 scenes. The only exception was the subset of the reference data from southern Kyrgyzstan (study site U) delineating the landslides that occurred in April 2017. The landslides were detected based on Behling and Roessner (2017) and later manually corrected by us.

The compiled landslide inventory mainly consists of single events with varying landslide extents (e.g. tailings dam collapse in Brazil (study site A), ice-rock avalanche in Pakistan (study site Z1)). The reference dataset from Kyrgyzstan, Ireland, and Iran are only three examples where more than one landslide was reordered for the same event. The dataset contains landslide examples from different environmental and climatic settings. Also, most of the landslides are rainfall-triggered.

2.2. Sentinel-1 data

We use SAR data acquired by C-band SAR sensors onboard Sentinel-1 A/B satellites, which are radar satellite missions operated by the European Space Agency (ESA) in the frame of the European Union's Copernicus Programme. From their launch to orbit on the 3rd April, 2014, and 25th April, 2016, they acquired images of the same area every 12 days worldwide. When both satellites were operational in orbit, it was possible to acquire SAR images with a repeat cycle of up to 6 days. Due to its all-weather imaging capability and high spatial-temporal resolution, Sentinel-1 data is extensively tested for landslide mapping tasks and has demonstrated good results in delineating the landslide extent (e.g. Figure 2).

For each landslide event, we selected three pre- and three post-event Sentinel-1 Interferometric Wide Swath Single-Look-Complex (SLC) scenes. In total, 252 SLC scenes were downloaded from Copernicus Data Space Ecosystem.² In most landslide cases, the scenes were available only on ascending or descending data acquisition modes. For the cases, where both data acquisition modes were available, we selected the dataset that was

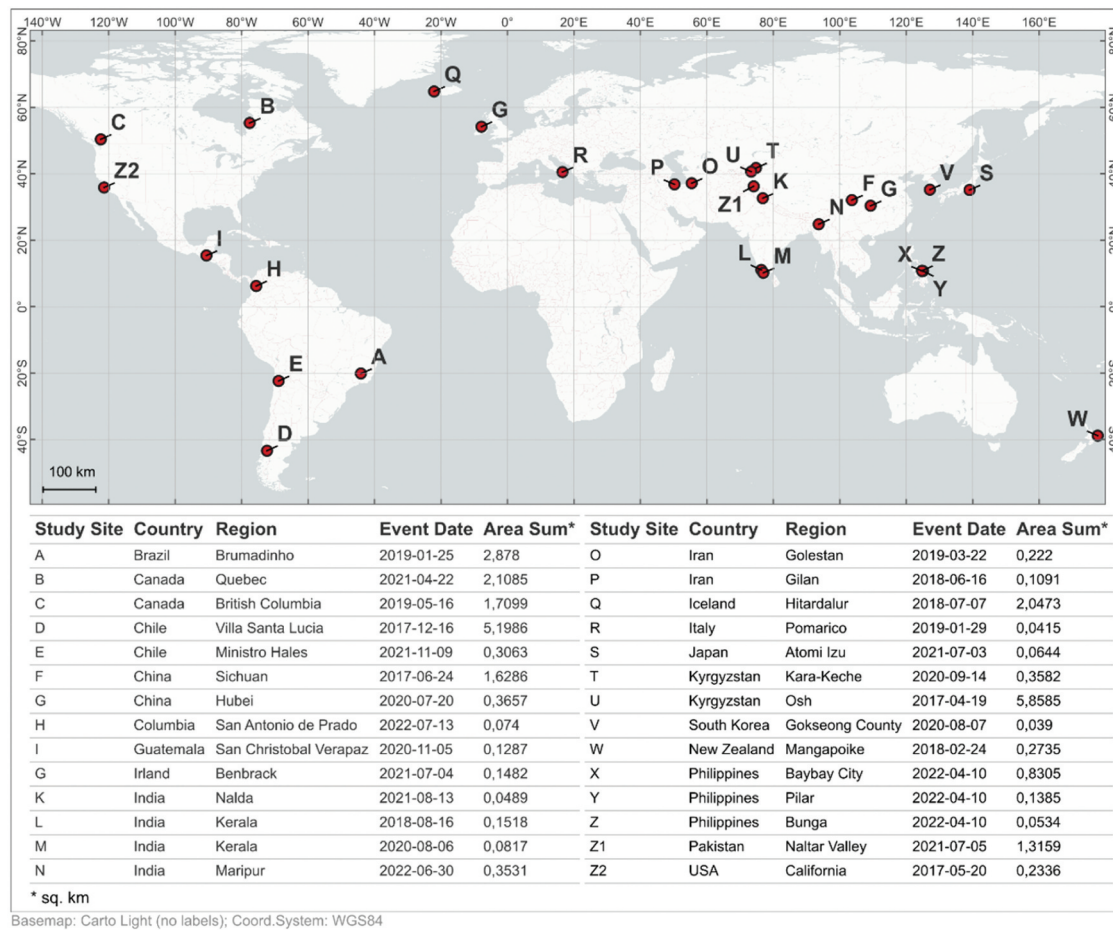


Figure 1. Spatial distribution of landslide events (map) and corresponding meta-information (Table).

most favorable concerning slope visibility where the landslide has happened. The list of all Sentinel-1 SLC scenes used in the study is provided as Supplementary Material 1.

One of the study objectives is to examine the utility of interferometric coherence and polarimetric decomposition features such as entropy, alpha angle, and anisotropy ($H/A/\alpha$) in addition to more commonly used radar backscatter coefficient data (VV, VH in gamma nought). Considering this, we run three pre-processing chains using the Graph Processing Tool (GPT) of ESA's Sentinel Application Platform (SNAP) software in version 9.0.0. For terrain correction, we used the digital elevation model (DEM) from Copernicus DEM (European Space Agency, Airbus 2022).

2.3. Sentinel-2 data

As an optical remote sensing data source, we used data acquired from the optical satellites Sentinel-2 A/B of ESA's Copernicus Programme (Figure 2). The data has been openly available for public use since

late 2015 (launch of Sentinel-2 A) and provided global coverage with 10 m spatial resolution for visible (RGB) and near-infrared (NIR) bands, 20 m for four red-edge (RE (1–4)), two short-waves near-infrared (SWIR (1–2)) bands. The launch of Sentinel-2 B in 2017 the repeat cycle was increased in some areas of the globe to 5 days.

For each landslide event, we selected one pre- and one post-event cloud- and cloud-shadow-free optical scene, totaling 56 scenes. We have selected only one scene before and after the landslide event due to the high variability in the availability of cloud-free scenes (Figure 3). While for some study sites, it was possible to find cloud-free scenes directly after or before the landslide (e.g. landslide in Kara-Keche region, Kyrgyzstan) for others the difference between pre-/post-event scenes could reach up to 6 months (e.g. fatal landslide in Sichuan province, China). The list of all Sentinel-2 scenes used in the study is provided as Supplementary Material 1.

To access Sentinel-2 data, we used Microsoft's Planetary Computer platform (Microsoft Open Source et al. 2022), a cloud-based platform that provides access to a wide

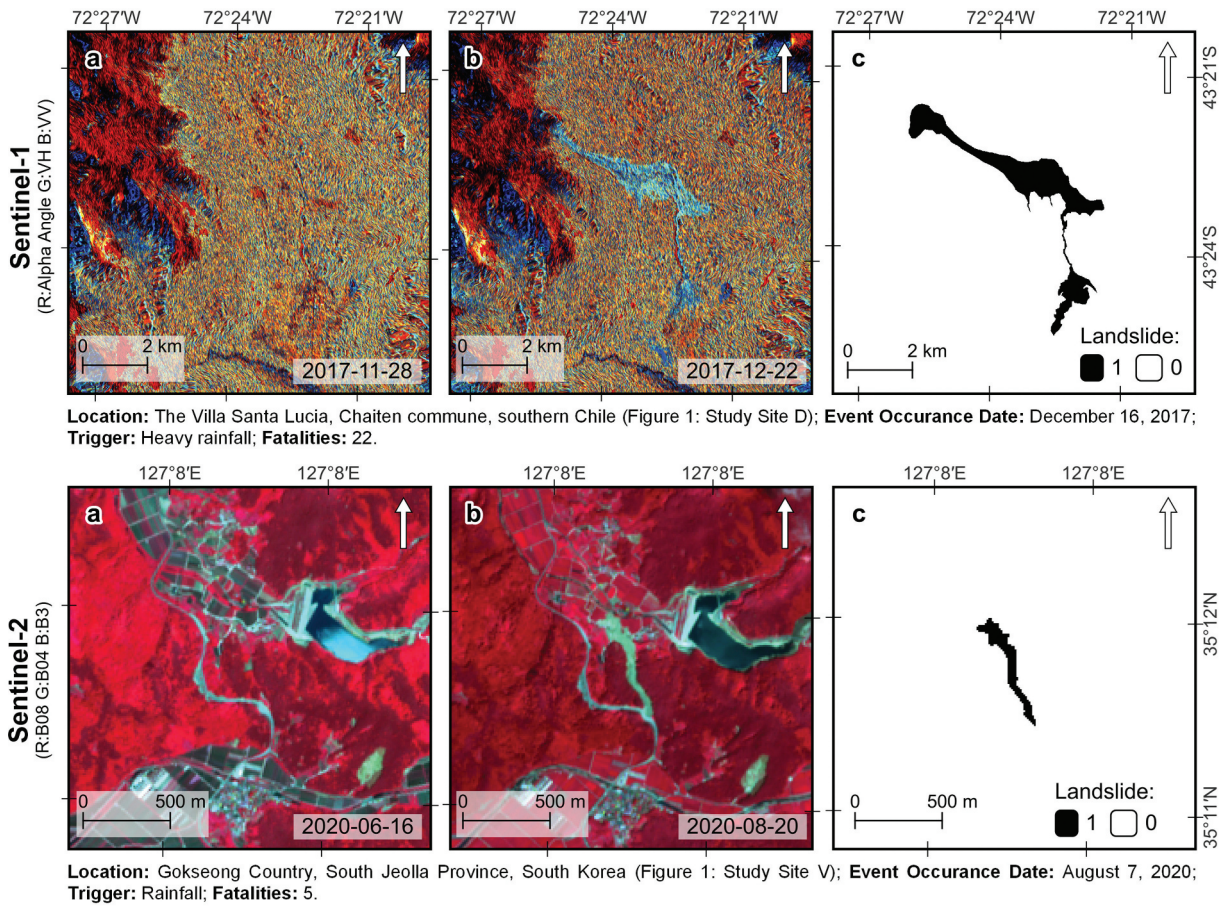


Figure 2. (a) Pre- and (b) post-event Sentinel-1 and Sentinel-2 data with (c) binary masks of landslide events from our inventory.

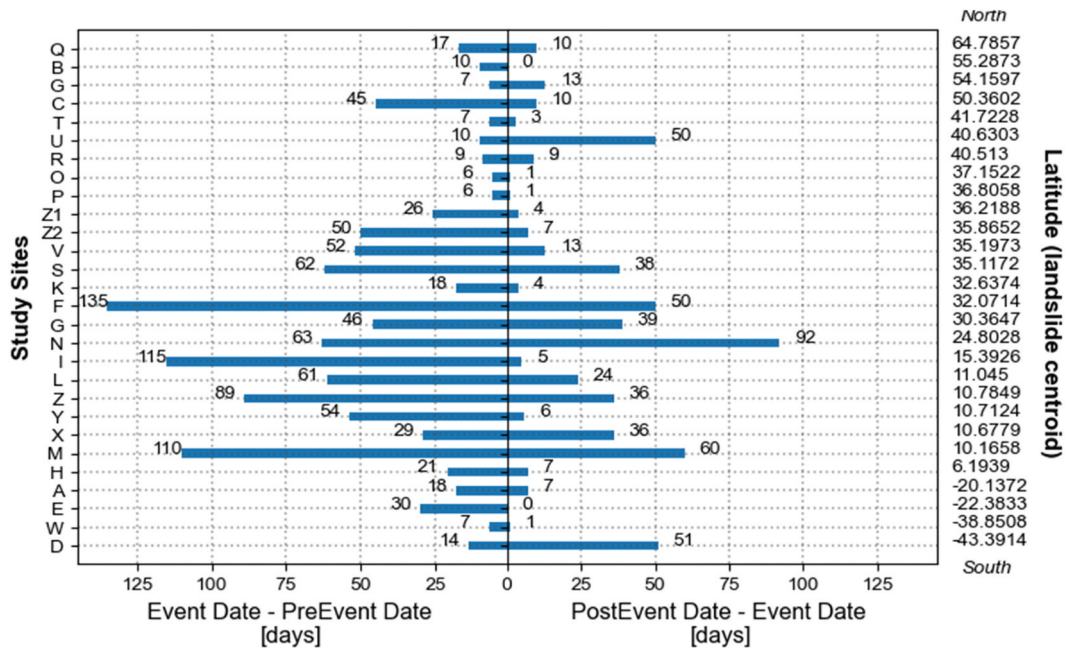


Figure 3. Number of days between event occurrence date and acquired pre- and post-event Sentinel-2 scenes.

range of geospatial datasets for research and analysis. The dataset was accessed through the STAC API by providing the predefined image acquisition date and area of interest.

2.4. Surface elevation and slope angle data

As one of the significant factors influencing the landslide generation (Wang et al. 2025), DEMs contribute valuable structural information about the landscape. Slope, derived from DEMs, further enriches the model by providing a quantitative measure of terrain steepness, which deep learning algorithms can exploit to distinguish landslide-affected areas from surrounding stable terrain, even in visually ambiguous scenes. Recent studies confirm (Ghorbanzadeh et al. 2019; Sameen and Pradhan 2019; Soares et al. 2020) that elevation and slope are not just supporting information but play an active role in improving the precision and reliability of deep learning-based landslide detection. By embedding terrain awareness into model training, these features help resolve ambiguities in complex terrain, ultimately leading to more trustworthy and scalable landslide mapping solutions.

We retrieved the DEM layers in meters for each landslide event from the publicly available Copernicus DEM dataset (Soares et al. 2022). Based on these DEM data, we calculated slope angle layers using gdaldem tool (Figure 4).

3. Methods

3.1. Reference data preparation and train-test split

For effectively training a semantic segmentation model such as U-Net, it is essential to have good-quality annotated data with corresponding feature vectors. For each

landslide event, we created a binary raster mask indicating the spatial allocation of the landslide and non-landslide pixels using the earlier described landslide inventory. As a feature vector, we used the varying combination of Sentinel-2 and Sentinel-1 features. More details on the feature combinations are provided in the following section. All input features were harmonized by resampling them to 10 m spatial resolution, re-projecting, channel-wise normalization, and clipping to the extent of the area of interest of each landslide event (Figure 5).

Since the size (height \times width) of the input Sentinel-1 and Sentinel-2 features are too large to feed them directly into the DL network and due to their varying spatial extents, we split the input features into smaller equalized patches of the size 128×128 pixels. The patch size was selected based on the reports from the earlier studies that suggested that the models trained with a patch size of 128×128 pixels (compared to, e.g., 32×32 pixels, 64×64 pixels) show higher classification accuracies (Ghorbanzadeh et al. 2021; Meena et al. 2022). Some studies have also reported that the models trained with larger patch sizes tend to have higher precision and lower recall rates (Prakash, Manconi, and Loew 2021; Soares et al. 2020, 2022).

After tiling the features from each landslide into smaller patches we had in total of 563 patches, which were then split at landslide event level to 80% for model training and validation and 20% for model testing. In the landslide mapping literature, the splitting of reference data to training and testing samples is often done randomly (Ghorbanzadeh et al. 2019; Nava et al. 2022) or using spatial blocks (Liu et al. 2020; Prakash, Manconi, and Loew 2020; Z. Yang and Xu 2022). This implies that data from the same landslide event appear in training and testing data. Such scenarios are unrealistic in real-world

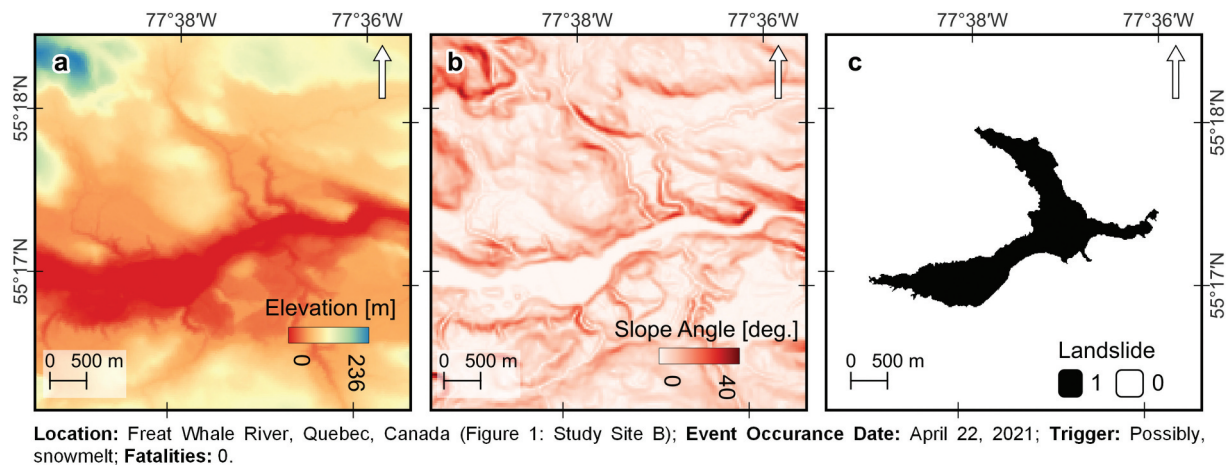


Figure 4. (a) Elevation and (b) slope angle layers from the landslide event in Canada.

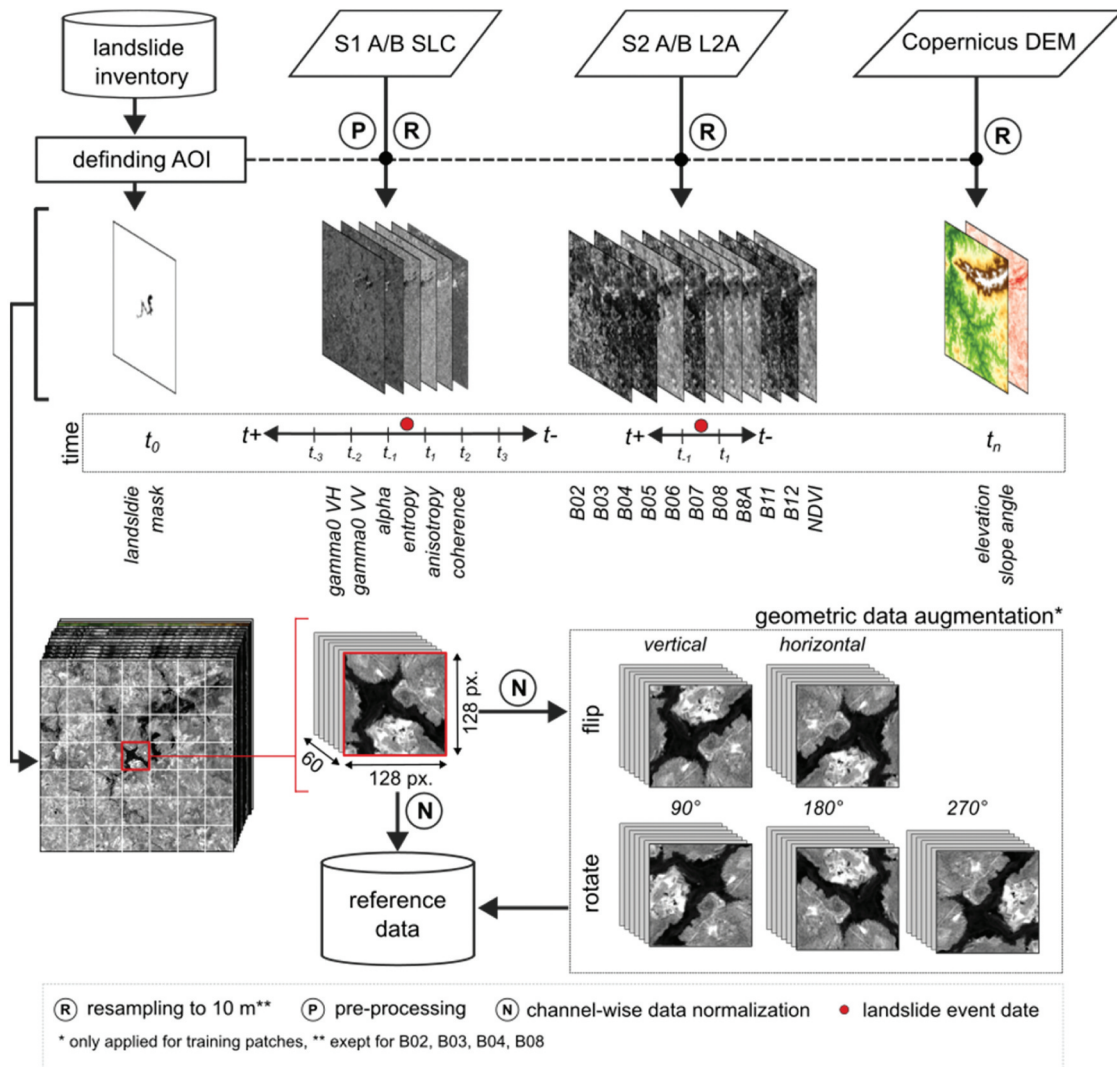


Figure 5. Generation of the landslide reference data for deep learning application.

applications, where training data for target landslides, even in insignificant amounts, are not available. Typically, machine learning or statistical models are trained using labeled data from previous landslide events, which are often environmentally and geographically dissimilar to the target event, and then spatially and temporally transferred to predict the new unseen dataset. To mimic such real-world scenarios but also to test the commonly applied “spatial block split” approaches (Roberts et al. 2017), we created two test sample sub-groups: (a) “*independent patches*” – image patches from four landslide events that are spatially and temporally independent from the training data and only were used for model testing; (b) “*dependent patches*” – image patches from four landslide events, where one part of the landslide patch samples was used for model training and the other part for model testing (Figure 6). Here, a “spatial

block split” was applied to ensure that there is no spatial overlap between training and testing patches.

According to earlier studies on landslide mapping using deep learning models (Cai et al. 2021; Yi and Zhang 2020, p.), increasing the number of training patches using image augmentation methods improves the predictive performance of the models. However, as Nava et al. (2022) have pointed out, augmentation of SAR data should be done with caution, since the unfavorable slope orientation to the sensor’s image acquisition geometry could increase the number of inconsistent data that decreases model performance. In our study, to increase the number of training patches, we applied geometric image augmentation techniques such as image flipping (horizontal and vertical) and image rotation (90°, 180°, and 270°). This helped us to increase the size of training patches to 2130.

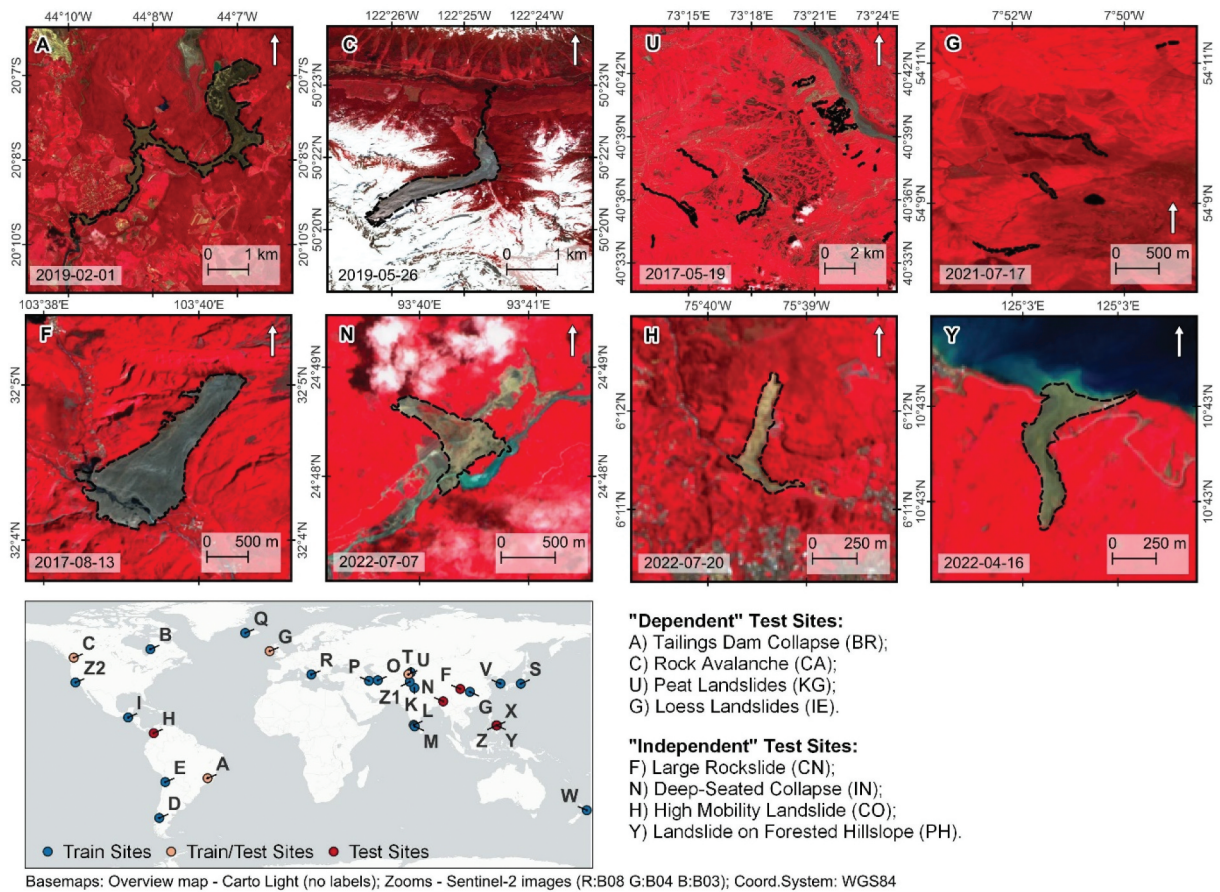


Figure 6. Overview of the independent and dependent test sites.

3.2. Input feature groups

In total, we ran 58 experiments with different sets of feature combinations from only optical, only SAR and a combination of both with four scenarios of data availability. (The graphical overview of the general study workflow is provided as Supplementary Material 2.) First, we grouped the feature combinations based on their sensor origin to understand if the usage sensor dataset shows superior performance compared to others (Table 1). Second, we set the most used feature combinations such as backscatter coefficients at VV and VH polarizations from SAR data or a combination of RGB and NIR bands from optical features as a base and started including other feature groups (e.g. H/A/ α , RE (1–4)) to evaluate the performance of the models with and without additional features. All feature combinations included elevation and slope angle features as standard topographic inputs, based on their demonstrated relevance in previous landslide detection studies (e.g. Sameen and Pradhan 2019).

3.3. U-Net Model

For a supervised automated classification task, we selected a convolutional neural network (CNN) model designed for semantic image segmentation tasks – U-Net (Ronneberger, Fischer, and Brox 2015). The U-Net model has gained significant attention in recent years due to its advanced performance compared to other machine learning classifiers in various application domains, and also among landslide classification studies (Ganerød et al. 2023; Konishi and Suga 2019; Nava et al. 2022; Lei et al. 2019). The U-Net architecture consists of an encoder-decoder part with skip connections (Figure 7). The encoder path captures the contextual information by progressively down-sampling the input images through convolutional and pooling layers. On the other hand, the decoder path up-samples the features and reconstructs the spatial information, enabling precise localization of objects of interest. The skip connections between the corresponding encoder and decoder parts allow the U-Net model to retain fine-grained

Table 1. List of the combination of features and a number of pre-/post-event scenes. All combinations also include slope angle and elevation features.

Satellite	Features	Number of pre-/post-event scenes			
		1 pre- + 1 post-event (1+1)	3 pre- + 1 post-event (3+1)	1 pre- + 3 post-event (1+3)	3 pre- + 3 post-event (3+3)
Sentinel-1	gVV+gVH	x	x	x	x
	gVV+gVH, COHVV	x	x	x	x
	gVV+gVH, H/A/ α	x	x	x	x
	gVV+gVH, COHVV, H/A/ α	x	x	x	x
Sentinel-2	RGB, NIR	x			
	RGB, NIR, NDVI	x			
	RGB, NIR, RE (1–4)	x			
	RGB, NIR, SWIR (1–2)	x			
	RGB, NIR, RE (1–4), SWIR (1–2)	x			
	NDVI	x			
Sentinel-1 + Sentinel-2	gVV+gVH, RGB, NIR	x*	x*	x*	x*
	gVV+gVH, NDVI	x*	x*	x*	x*
	gVV+gVH, RGB, NIR, RE (1–4), SWIR (1–2)	x*	x*	x*	x*
	gVV+gVH, COHVV, RGB, NIR	x*	x*	x*	x*
	gVV+gVH, COHVV, NDVI	x*	x*	x*	x*
	gVV+gVH, COHVV, RGB, NIR, RE (1–4), SWIR (1–2)	x*	x*	x*	x*
	gVV+gVH, H/A/ α , RGB, NIR	x*	x*	x*	x*
	gVV+gVH, H/A/ α , NDVI	x*	x*	x*	x*
	gVV+gVH, H/A/ α , RGB, NIR, RE (1–4), SWIR (1–2)	x*	x*	x*	x*
	gVV+gVH, COHVV, H/A/ α , RGB, NIR, RE (1–4), SWIR (1–2)	x*	x*	x*	x*

*pre- and post-event scenes change only for features based on Sentinel-1 scenes.

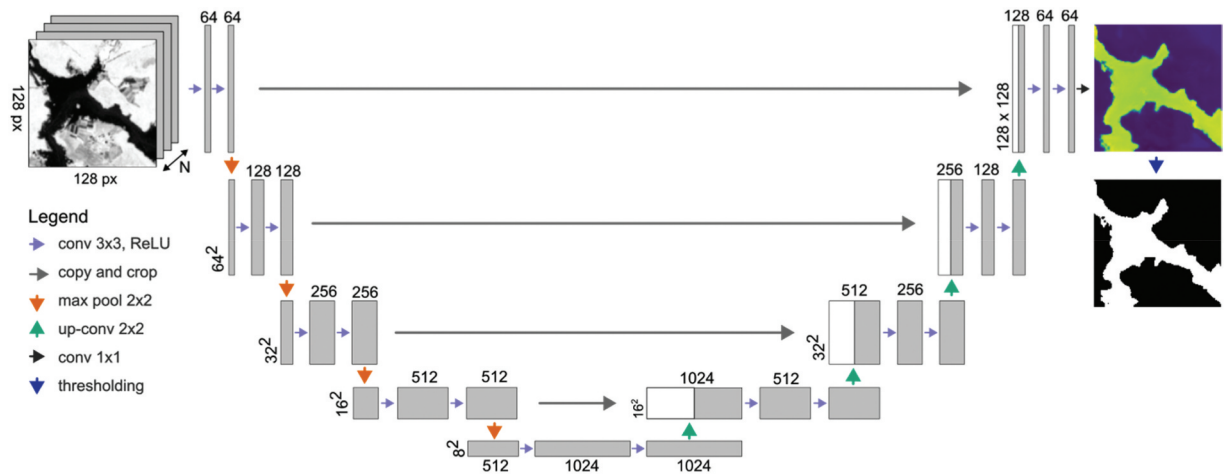


Figure 7. U-Net architecture used in this study.

details during the up-sampling, facilitating accurate segmentation. This feature is particularly advantageous when dealing with complex or irregularly shaped objects in an image, such as landslides.

In our U-Net architecture, the encoder part processes the input patches through five convolutional blocks which extract the features at different scales. Within each convolution block, two 3×3 convolutions with Rectified Linear Unit (ReLU) activation are applied that is followed by batch normalization. The block concludes with a max pooling operation with a kernel size of 2×2 , which downsizes the feature maps by a factor of 4. However, the number of feature channels is doubled after each block. In the decoder part of the architecture, the feature maps are up-sampled to

match their original input dimension. Similarly, the encoder part is done through five convolutional blocks. Each block comprises a 2×2 transpose convolution that reduces the number of feature channels by half. The resulting output is then concatenated with the corresponding feature map encoder part. Following this concatenation, two 3×3 convolutions with ReLU activation are applied, each subsequently normalized using batch normalization. The final layer of the architecture consists of a 1×1 convolution with sigmoid activation, which results in a landslide probability layer. To get a binary landslide, non-landslide output mask, we apply a threshold of 0.5 to the probability layer. In this study, we utilized the “same” in all convolutional layers of the U-Net model to ensure that the spatial dimensions of

the input images are preserved, thereby avoiding the introduction of artifacts associated with zero-padding at the edges.

The U-Net model was trained with augmented training patches described in Section 3.1. All the input patches were scaled from 0 to 1 at the individual channel level before feeding them to the network. Considering the computational constraints and memory limitations, we selected a moderate batch size of 16 patches with a total of 200 epochs. With a low learning rate of 0.0001, we aimed to cautiously update the model parameters, preventing the drastic changes that may hinder convergence. The soft dice criterion was chosen as our loss function, as it effectively measures the similarity between the predicted and ground truth segmentation masks. Overall, these parameter choices were made based on their compatibility with our dataset and task requirements, aiming to optimize the performance of the U-Net architecture in our specific context.

3.4. Performance evaluation

In our study, the landslide classification accuracies were evaluated using two test sets – independent and dependent. Each of the test sets consists of patches from four separate landslide events. We report accuracies for each landslide but also group into independent and dependent test sites to address the question of spatial-temporal independence of the test samples.

$$precision = \frac{True\ Positive}{True\ Positive + False\ Positive} \quad (eq.1)$$

$$recall = \frac{True\ Positive}{True\ Positive + False\ Negative} \quad (eq.2)$$

$$F1 - score = 2 * \frac{precision * recall}{precision + recall} \quad (eq.3)$$

$$IoU = \frac{Area\ of\ Overlap}{Area\ of\ Union} \quad (eq.4)$$

We selected the most frequently used metrics among landslide classification studies – precision (eq. 1), recall (eq. 2), F1-score (eq. 3), and Intersection over Union (IoU) (eq. 4). This would ensure comparability to other studies. All metrics have a range of values between 0 and 1, with higher values indicating superior performance.

4. Results

4.1. Landslide classification accuracies

As it was anticipated, the classification metrics significantly vary across eight test sites (Figure 8). For some test sites, we acquired high accuracies (F1-score above 0.75) with all possible feature combinations (e.g. Tailing Dam Collapse in Brazil, Large Rockslide in China), whereas for others, no landslide pixels were detected (e.g. Peat Landslide in Ireland) or only with specific sensor data (e.g. Deep-Seated Collapse in India, High Mobility Landslide in Colombia). The last three landslides are below 0.5 km² in size.

The highest F1-score of 0.96 was reached when mapping the Large Rockslide in China using optical features. Whereas the lowest classification accuracy (F1-score of 0) was recorded when mapping Peat Landslides in Ireland with optical features and High Mobility Landslide in Colombia using SAR features. This occurred due to the total absence of correctly predicted landslide pixels (i.e. True Positives). On average, the model outcomes showed higher precision and lower recall values across all test sites (see Supplementary Material 3).

The difference between F1-scores derived from dependent and independent test sites was most noticeable when using only SAR features. The F1-score values across all combinations of SAR features were on average lower (Δ 0.21) for independent test sites compared to dependent test sites. In contrast, for only optical and optical-SAR combinations, the average accuracies were slightly higher for independent test sites (Δ 0.12 and Δ 0.09, respectively). When excluding the accuracies based on Peat Landslides (dependent test site), which showed extremely poor results, the average accuracies of dependent test sites across all three sensor combinations show higher values compared to those derived from independent test sites (Δ 0.21 for SAR, Δ 0.05 for optical and Δ 0.08 for combination). Also, the variability of classification accuracies with different sets of feature combinations within one sensor data is much higher in independent test sites compared to dependent test sites (Figure 8).

4.2. Optical, SAR, and their combination

The highest F1-score was systematically reached using only optical features across all test sites except for the Deep-Seated Collapsed in India (Figure 9). The highest average F1-score of 0.83 was reached using RGB, NIR with SWIR bands combination across all eight test sites. However, when calculated separately, for independent test sites the highest average accuracies (F1-score of 0.87) were reached using NDVI bands alone. The

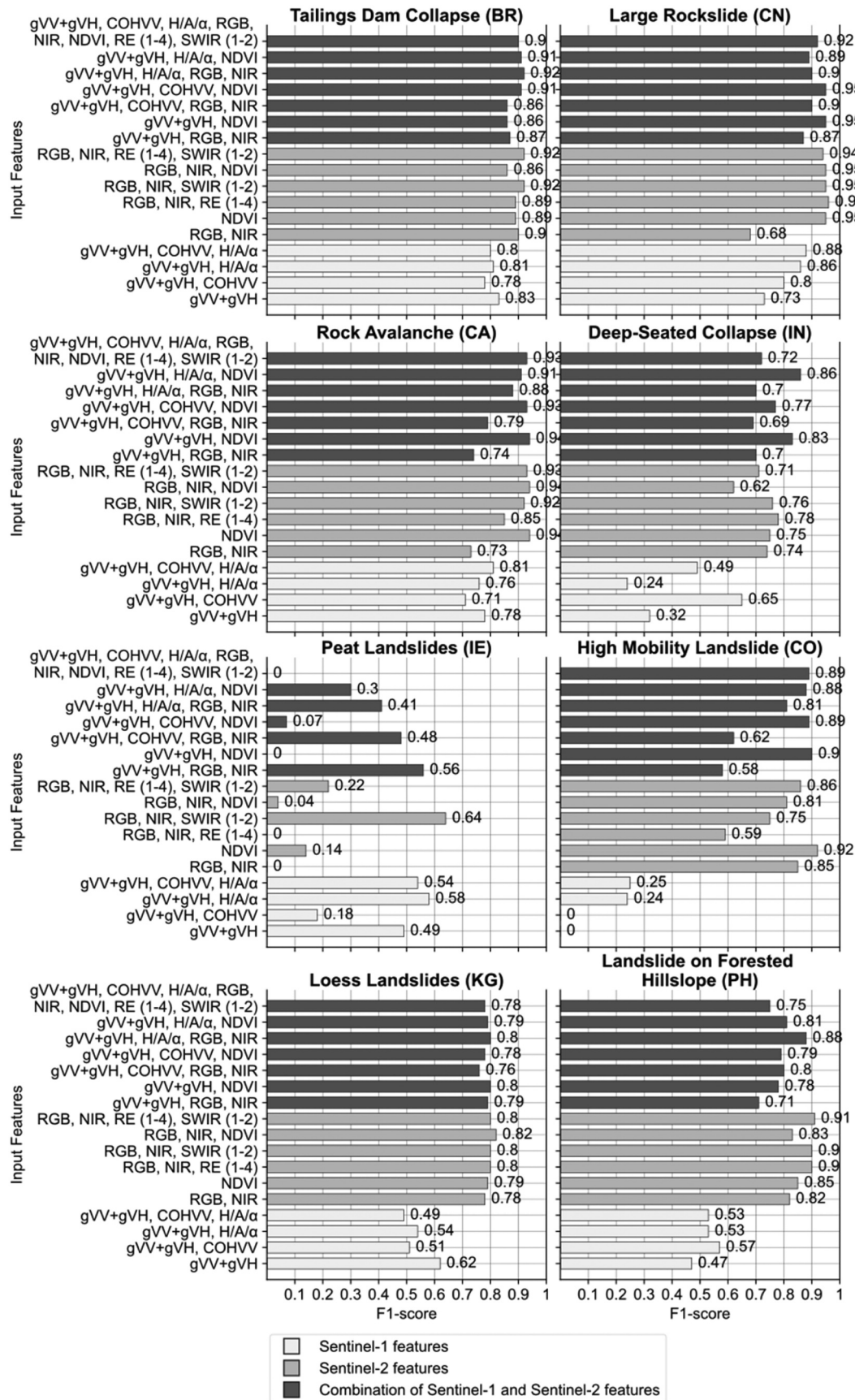


Figure 8. Classification accuracies (y-axis) across four dependent (first row) and four independent (second row) test sites using only optical, only SAR and a combination of optical and SAR features (colour) for one pre-/post-event. The corresponding values of precision, recall, and IoU can be found in Supplementary Material 3.

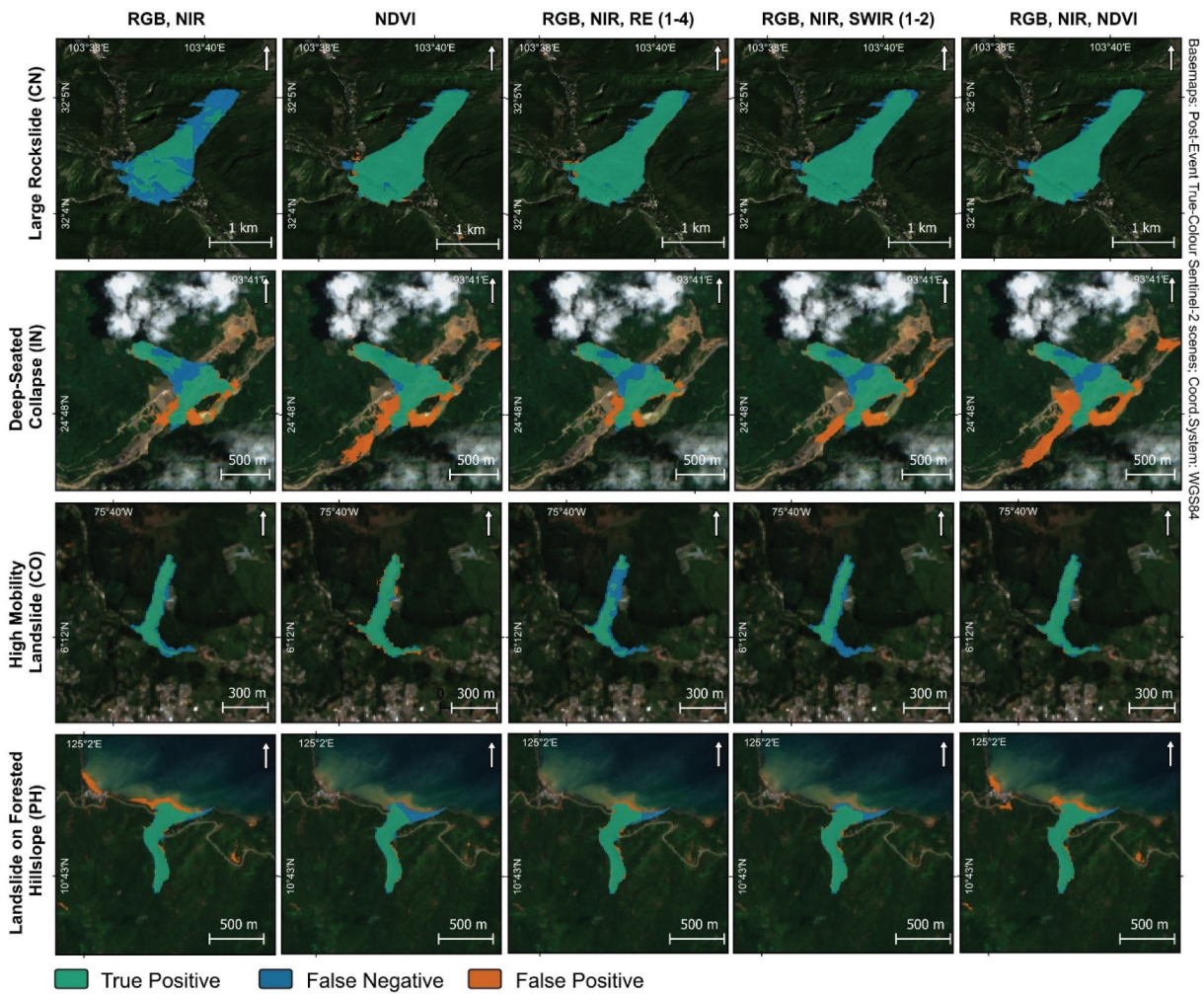


Figure 9. Landslide classification maps with different sets of optical features (columns) for independent test sites (rows). A corresponding map for dependent test sites is available as Supplementary Material 4.

combination of RGB and NIR bands, which are most commonly used among landslide mapping studies, showed the lowest average performance (F1-score 0.69) for runs with only optical features. The addition of four RE bands to RGB and NIR bands showed a minimal increase in the accuracies (F1-score Δ 0.03) compared to using RGB, and NIR alone.

The lower performance of RGB and NIR bands compared to other optical band combinations was mainly due to the higher recall and low precision (see Supplementary Material 4). The landslides that occurred in densely vegetated areas (e.g. in Colombia and the Philippines) were well mapped using only NDVI data or a combination of RGB, NIR, and NDVI.

The low or high number of days between pre-event and post-event cloud-free scenes does not seem to correlate with the classification results (Figures 3 and 8). The shortest time difference of 20 days between pre-/post-event scenes for Peat Landslides in Ireland (low

classification accuracies) and the biggest difference of 185 days was recorded for Large Rockslide in China (highest classification accuracies).

Among runs based on only SAR features, the highest average accuracies (F1-score 0.60) across all test sites were reached when all SAR features were used to train the model. However, when averaged separately, the highest accuracies for dependent test sites were reached using gVV + gVH (F1-score 0.68) and with all features (F1-score 0.54) for independent test sites.

The models based on SAR data showed satisfactory classification accuracies (F1-score above 0.70) when mapping larger landslides (e.g. Large Rockslide in China, Tailings Dam Collapse in Brazil) but often failed to accurately predict smaller landslides (e.g. Peat Landslides in Ireland, High Mobility Landslide in Colombia) and landslide with more complex geometry (e.g. Loess Landslides in Kyrgyzstan). Apart from the size of the landslides, the surrounding landscape topography

also had a negative effect on the SAR-based model performance. Mapping the narrow structures of Dam Tailings Collapse in Brazil (narrow mudflow runway through the forested area) and Rock Avalanche in Canada (deep river channel) was not feasible (Figure 10).

The combination of optical and SAR features (gVV + gVH, H/A/ α , NDVI) showed higher performance compared to only optical or only SAR features in Deep-Seated Collapse in India (F1-score 0.85). However, the F1-score difference to the best-performing optical features (RGB, NIR, RE) was Δ

0.08. Among all test sites, the highest accuracies were reached when radar backscatter and polarimetric features were combined with NDVI (average F1-score of 0.79). While the classification accuracies of the optical-SAR combination were always higher than only SAR-based results, they were also always below accuracies received from only optical runs.

Apart from the Peat Landslides in Ireland, the optical-SAR combination showed good mapping results for large as well as small landslides (Figures 11 and 12).

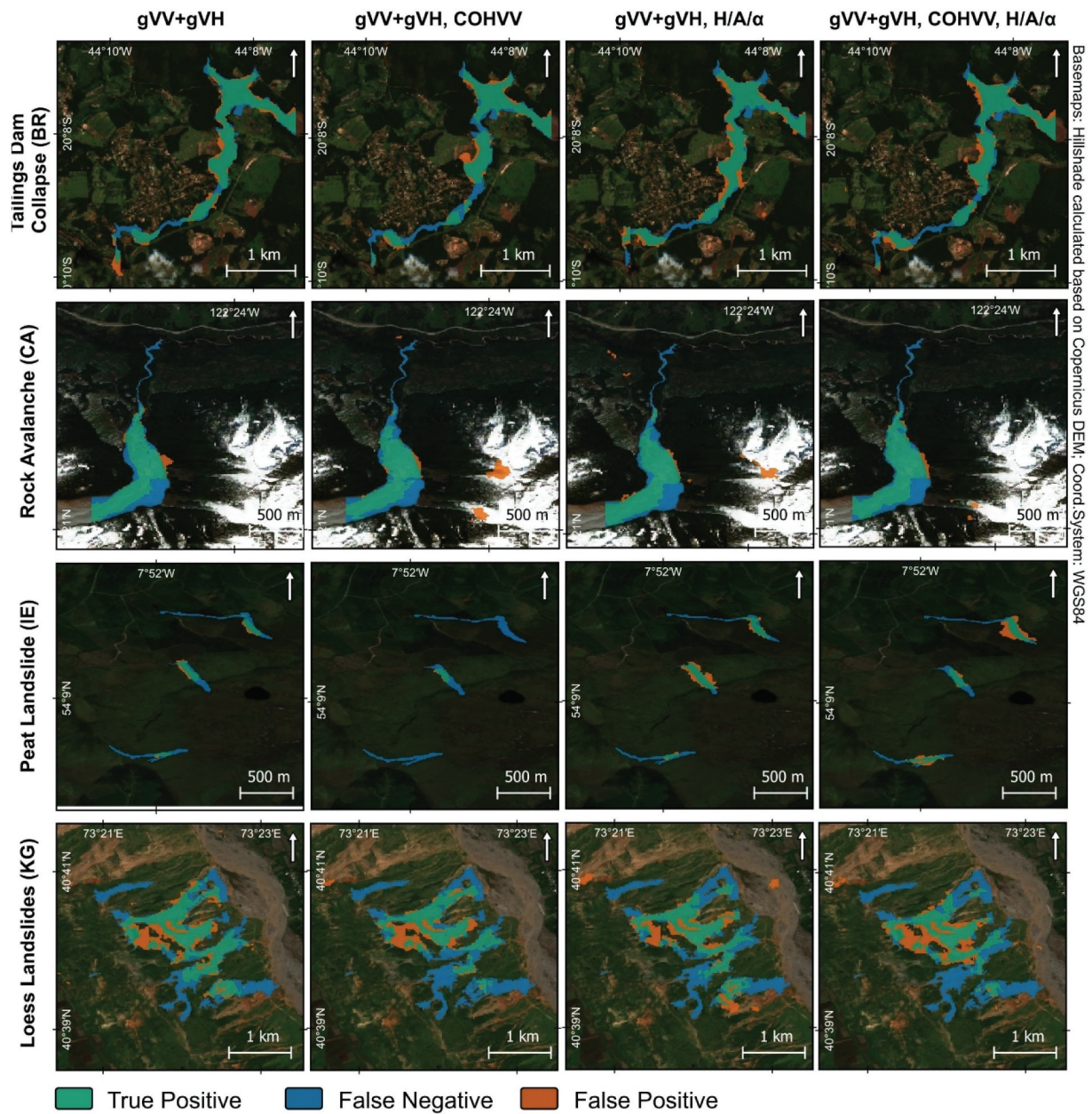


Figure 10. Landslide classification maps with different sets of SAR features (columns) for dependent test sites (rows). A corresponding map for independent test sites is available as Supplementary Material 5.

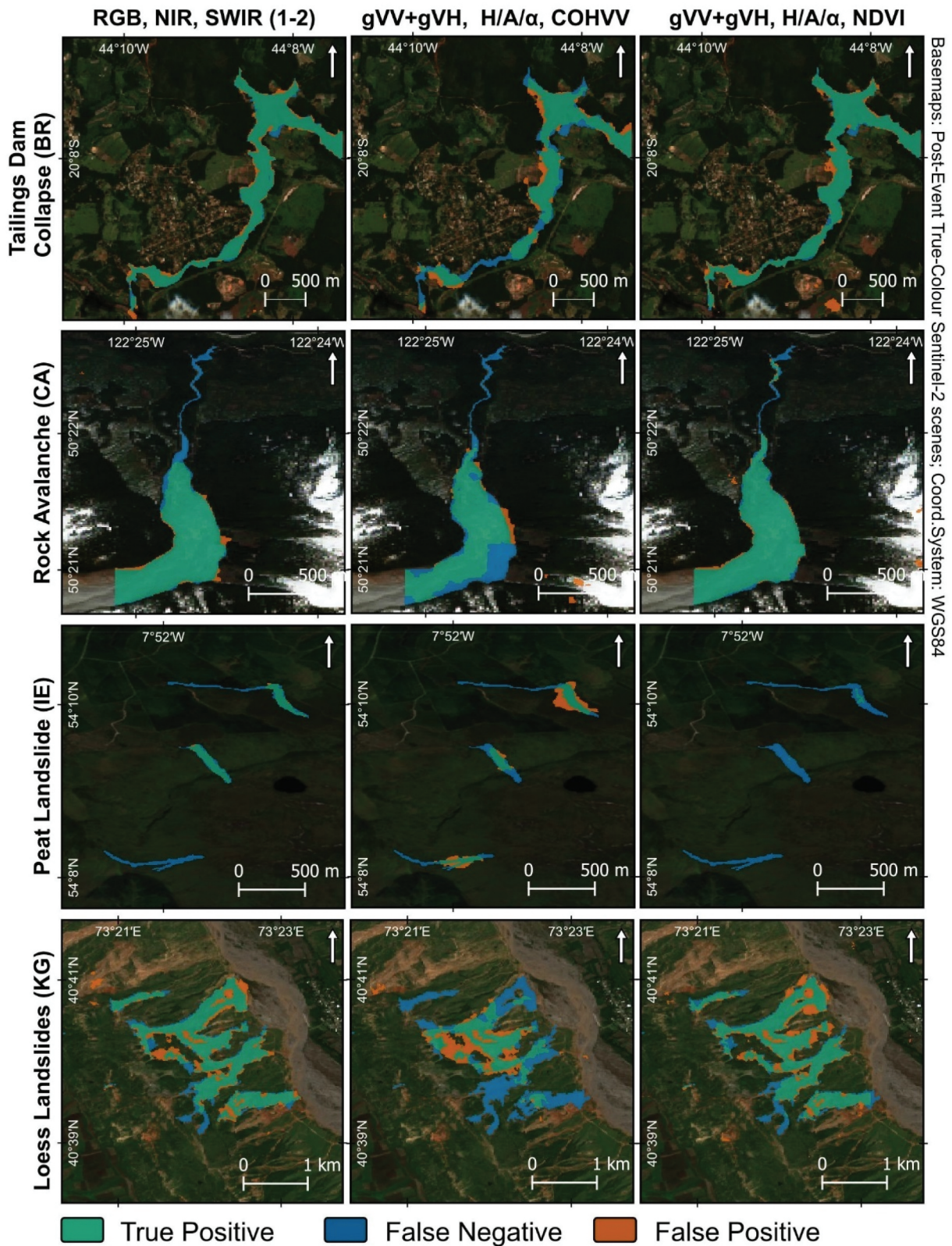


Figure 11. Landslide classification maps with best performing only optical only SAR and combination of optical and SAR features for dependent test sites.

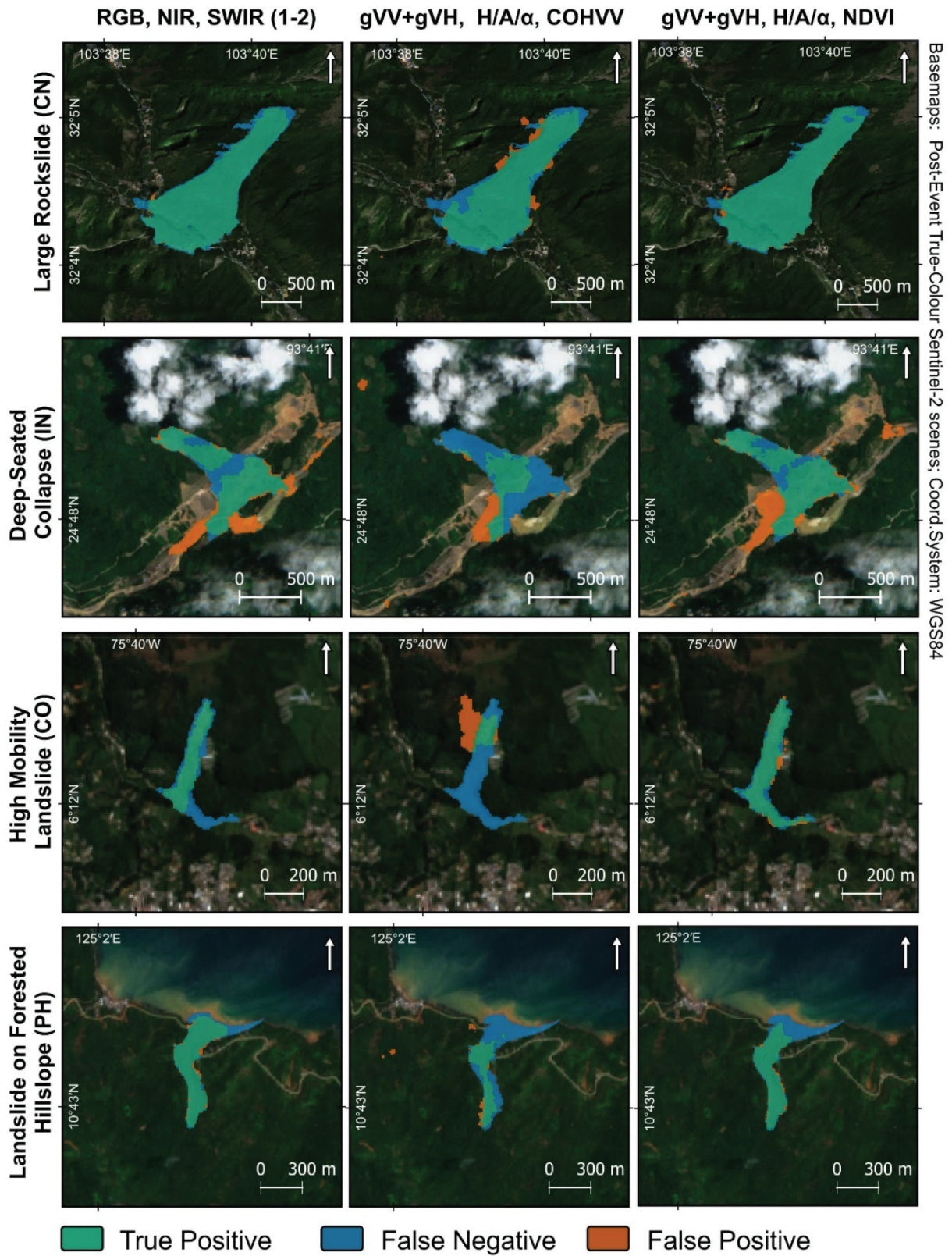


Figure 12. Landslide classification maps with best performing only optical only SAR and combination of optical and SAR features for independent test sites.

4.3. Impact of multi-temporal SAR inputs

We observed a consistent improvement in classification accuracies when multiple pre-/post-event scenes were used for landslide mapping using only SAR features across all test sites (Figure 13). The most significant increase of F1-score (Δ 0.13) was recorded when three pre-event and three post-event scenes were used to map the Landslide on the Forested Hillslope. The lowest increase in F1-score (Δ 0.02) was recorded when three pre-event and three post-event scenes were used to map the Deep-Seated Collapse in India. However, despite the overall increase, the classification accuracies based on only SAR data did not reach the highest accuracies derived from only optical features for corresponding test sites (Figure 8).

5. Discussion

The outcomes of our study illustrate that U-Net can achieve promising accuracies in landslide mapping, even when trained on limited datasets, aligning with the findings of Meena et al. (2022) and Prakash, Manconi, and Loew (2020). However, the landslide-specific accuracies varied significantly depending on the complexity of the cases. Large landslides, such as the Large Rockslide in China or Tailings Dam Collapse in Brazil, achieved F1-scores exceeding 0.9. In contrast, smaller or geometrically complex landslides, such as Peat Landslides in Ireland or Loess Landslides in Kyrgyzstan, posed greater challenges, resulting in lower accuracies. These findings highlight the importance of accounting for the diverse characteristics (e.g. type, size, and shape) of landslides when building deep learning models and underscore the necessity for diverse training datasets with various landslide types, topographies, shapes, and geo-environmental conditions in order to enhance model's generalizability and robustness.

The study results show that optical features consistently outperformed SAR features and their combination across all test cases. This finding aligns with previous studies by Nava, Monserrat, and Catani (2022) and Jelének and Kopačková-Strnadová (2021), which emphasize the superior ability of optical data to detect vegetation cover change – one of the key indicators of landslides. The landslides analyzed in this study were primarily associated with the transition from dense or semi-vegetated land cover to bare soil or rock. This explains the higher performance of optical data, which is particularly effective in capturing vegetation cover changes. While SAR data offers the advantage of all-weather capabilities, its geometric distortions in mountainous regions, such as shadow, layover, and

foreshortening, can reduce landslide detection accuracy. Despite acceptable average accuracies F1-score ≥ 0.7 , SAR data requires cautious use, particularly in topographically challenging areas. When optical data is available, it should be prioritized over SAR data for landslide detection using U-Net. Before relying solely on SAR data, it is essential to thoroughly assess potential limitations, such as topographical complexity and unfavorable viewing angles, which may adversely impact detection accuracy.

The combination of optical and SAR features shows minimal accuracy benefits only in one (out of eight) landslide cases. We found no particular advantages of using the optical-SAR combination over only optical data with a deep learning approach. This finding contrasts with studies illustrating the utility of optical-SAR fusion in rule-based classification workflows (Plank, Twele, and Martinis 2016; Jelének and Kopačková-Strnadová 2021). Combining optical and SAR data also implies an increase in feature dimensionality. With limited training data, this could lead to reduced performance of the model due to the dimensionality curse. This suggests that, in deep learning-based approaches, the additional complexity introduced by optical-SAR data combination may not always yield significant improvements and could potentially hinder model performance when training data is scarce.

Among the run utilizing only optical features, the addition of SWIR bands to the conventional RGB and NIR combination consistently yielded the highest classification accuracies across eight test sites. SWIR bands capture valuable information on moisture content, mineral composition, and vegetation health, which are relevant factors in landslide mapping. These findings align with earlier studies, such as Lu et al. (2021), which demonstrated the utility of SWIR bands for mapping earthquake-triggered landslides in China and Japan. Therefore, incorporating SWIR bands with conventional RGB and NIR is strongly recommended for more accurate and comprehensive landslide mapping.

Our analysis revealed that increasing the number of pre- and post-event SAR scenes leads to improved classification in performance when using SAR-only inputs. This observation is consistent with the findings by Nava et al. (2022), where higher accuracies were reached with two post-event Sentinel-1 scenes compared to a single one. The advantage of multiple SAR scenes lies in their ability to capture changes over time, thereby providing a more comprehensive understanding of surface deformation and land cover transitions associated with landslides. In regions, where optical data is limited or unavailable due to adverse weather conditions, the use of multiple SAR scenes can significantly enhance the reliability of the model by compensating for the lack of optical data.

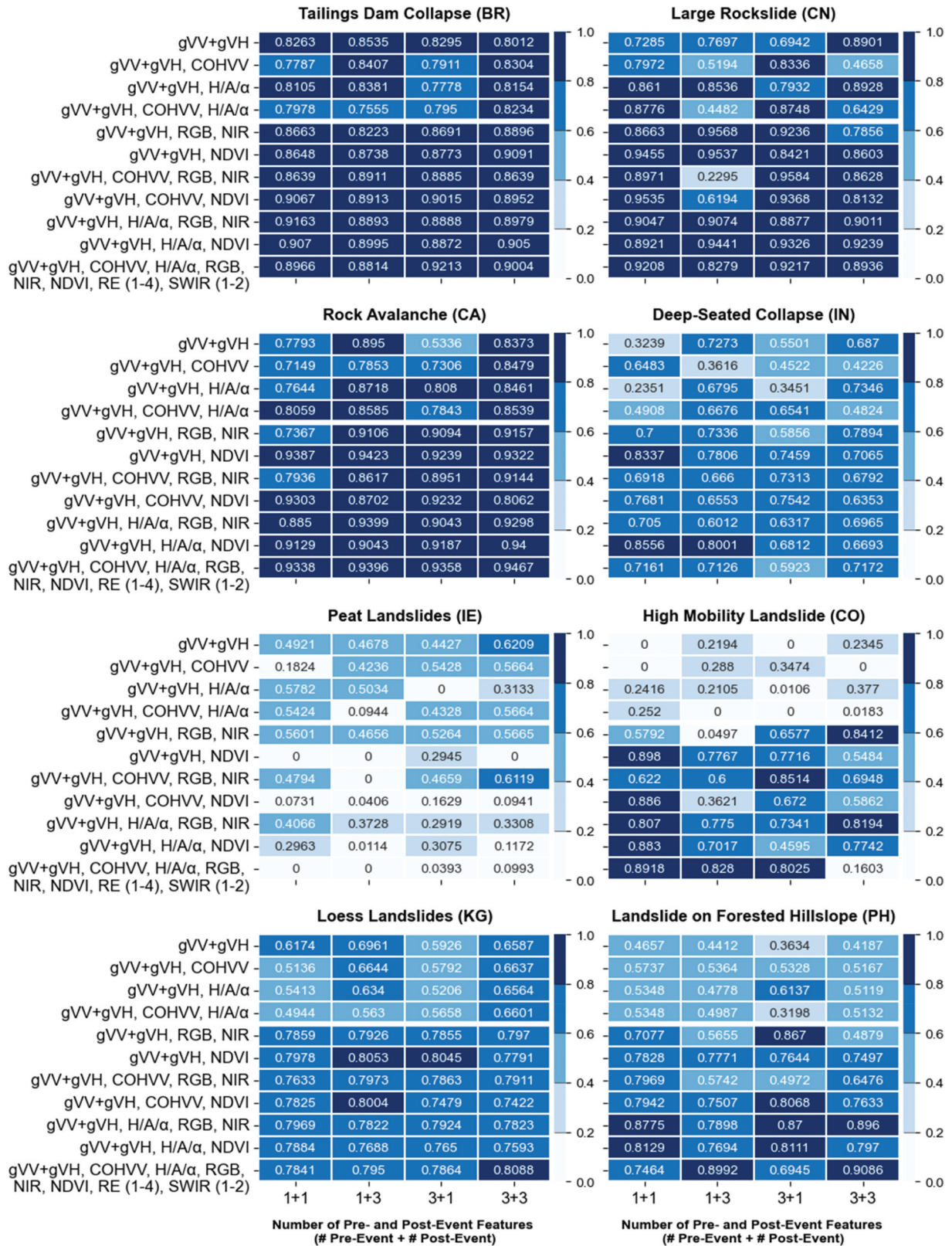


Figure 13. The F1-score values for dependent and independent test sites using a varying number of pre-/post-event scenes (x-axis) of only SAR features and optical-SAR feature combination (y-axis).

Ensuring the robustness of deep learning models for landslide classification across diverse geo-environmental settings remains a critical challenge. Testing the spatial-temporal transferability of ML/DL models is essential for real-world applications, where geographical and temporal settings may vary significantly. While our study did not show any substantial difference between independent and dependent test sets, the limited size of training and testing datasets could potentially be the major influencing factor. Future research should leverage larger and more diverse reference data to explore model transferability and generalizability more comprehensively.

A significant challenge in landslide mapping research is the limited availability of comprehensive, high-quality reference data. While benchmark datasets such as Landslide4Sense, CAS Landslide Dataset, and HR-GLDD provide a valuable foundation for exploring ML/DL models and training configurations, they often lack essential landslide-specific metadata, including georeferenced footprints and precise occurrence dates. This omission constrains geoscientific research and limits the integration of additional datasets, such as new sensor data or expanded temporal features. To address this gap, we openly share the dataset used in this study, which includes detailed georeferenced landslide footprints and associated metadata, via Zenodo (<https://doi.org/10.5281/zenodo.15284357>). We encourage future studies to adopt a similar approach by including landslide-specific metadata, thereby advancing the capabilities of the landslide mapping community.

When reflecting on the outcomes of this study, it is important to recognize and acknowledge the inherent limitations that may have influenced the results. The main limitation, as for many landslide studies, is limited reference data availability. It constrains model's ability to fully capture the variability of landslide types and environmental conditions, which could explain some variations in performance across different test cases. Another aspect is the type of considered landslide events. Our reference data mainly consists of the large and medium landslide events that occurred due to heavy rainfall. However, we do not have cases where one landslide event consists of many small landslides distributed over a large region, which is more common for earthquake-triggered landslide events. These limiting factors should be considered when evaluating the general applicability of the study.

6. Conclusion

Rapidly changing climate and the growing impact of human activities are expected to increase the occurrence

and mortality of landslide hazards. Applying deep learning techniques for landslide classification represents a significant stride in advancing our ability to accurately and efficiently monitor sites hit by this natural hazard. In this study, we explored the potential of Sentinel-1 and Sentinel-2 features, together and alone, for mapping landslides using the U-Net semantic segmentation model. With the limited but globally distributed landslide inventory, we tested how the various combinations of features, and the increased number of pre-/post-event SAR scenes could affect the classification accuracies. Based on the results of our study, the following conclusions can be inferred:

- The classification accuracies of U-Net models based on optical features consistently outperform those based on SAR features.
- No substantial accuracy improvements were found when combining optical and SAR features compared to results achieved with only optical data.
- The highest average classification accuracy, an F1-score of 0.83, was reached with RGB, NIR, and SWIR.
- The commonly used RGB and NIR band combination showed the lowest average performance across all test sets (F1-score 0.68) among only optical features.
- Increasing pre- and post-event scenes improved accuracies across all test sets when using only SAR features.

While optical data remains the most effective for accurate landslide mapping, SAR data shows potential for improvement with enhanced temporal resolution. Given the global distribution and limited nature of the reference data used in this study, further research with larger, more diverse datasets is needed to refine the applicability of SAR-based approaches for rapid landslide mapping.

Notes

1. <https://blogs.agu.org/landslideblog/>.
2. <https://dataspace.copernicus.eu/>.

Disclosure statement

No potential conflict of interest was reported by the author(s).

Funding

This study was funded by the Helmholtz Imaging Platform (HIP) project MultiSaT4SLOWS (Multi-Satellite Imaging for Space-based Landslide Occurrence and Warning Service). Helmholtz Imaging Platform (HIP).

ORCID

Simon Plank  <http://orcid.org/0000-0002-5793-052X>

Data availability statement

The remote sensing dataset used in this study has been made publicly available on Zenodo. It can be accessed via <https://doi.org/10.5281/zenodo.15284357>. This dataset includes georeferenced information on all 28 landslides used in this study and contain Sentinel-1, Sentinel-2 features along with slope angle and elevation layers. The dataset is provided under a Creative Commons Attribution 4.0 International (CC-BY-NC-4.0) license. Researchers are encouraged to use this dataset for further research, with appropriate citation of both the dataset and this paper.

References

- Behling, R., and S. Roessner. 2017. "Spatiotemporal Landslide Mapper for Large Areas Using Optical Satellite Time Series Data." In *Advancing Culture of Living with Landslides*, edited by M. Mikos, B. Tiwari, Y. Yin, and K. Sassa, 143–152. Cham: Springer International Publishing.
- Cai, H., T. Chen, R. Niu, and A. Plaza. 2021. "Landslide Detection Using Densely Connected Convolutional Networks and Environmental Conditions." *IEEE Journal of Selected Topics in Applied Earth Observations & Remote Sensing* 14:5235–5247. <https://doi.org/10.1109/JSTARS.2021.3079196>.
- Chen, L.-C., Y. Zhu, G. Papandreou, F. Schroff, H. Adam. 2018. "Encoder-Decoder with Atrous Separable Convolution for Semantic Image Segmentation." In: V. Ferrari, M. Hebert, C. Sminchisescu, Y. Weiss, (Eds.), *Computer Vision – ECCV 2018, Lecture Notes in Computer Science*. Cham: Springer International Publishing. pp. 833–851. https://doi.org/10.1007/978-3-030-01234-2_49.
- European Space Agency and Airbus Defence and Space GmbH. "Copernicus Digital Elevation Model (DEM) for Europe at 30 arc seconds (ca. 1000 meter) resolution derived from Copernicus Global 30 meter DEM dataset." 2022. Available: <https://doi.org/10.5281/zenodo.6211553>.
- Fichtner, F., N. Mandery, M. Wieland, S. Groth, S. Martinis, and T. Riedlinger. 2023. "Time-Series Analysis of Sentinel-1/2 Data for Flood Detection Using a Discrete Global Grid System and Seasonal Decomposition." *International Journal of Applied Earth Observation and Geoinformation* 119:103329. <https://doi.org/10.1016/j.jag.2023.103329>.
- Foody, G. M., A. Mathur, C. Sanchez-Hernandez, and D. S. Boyd. 2006. "Training Set Size Requirements for the Classification of a Specific Class." *Remote Sensing of Environment* 104 (1): 1–14. <https://doi.org/10.1016/j.rse.2006.03.004>.
- Froude, M. J., and D. N. Petley. 2018. "Global Fatal Landslide Occurrence from 2004 to 2016." *Natural Hazards and Earth System Sciences* 18 (8): 2161–2181. <https://doi.org/10.5194/nhess-18-2161-2018>.
- Fu, S., S. M. De Jong, X. Hou, J. de Vries, A. Deijns, and T. de Haas. 2024. "A Landslide Dating Framework Using a Combination of Sentinel-1 SAR and -2 Optical Imagery." *Engineering Geology* 329:107388. <https://doi.org/10.1016/j.enggeo.2023.107388>.
- Ganerød, A. J., E. Lindsay, O. Fredin, T.-A. Myrvoll, S. Nordan, and J. K. Rød. 2023. "Globally Vs. Locally Trained Machine Learning Models for Landslide Detection: A Case Study of a Glacial Landscape." *Remote Sensing* 15 (4): 895. <https://doi.org/10.3390/rs15040895>.
- Ghorbanzadeh, O., T. Blaschke, K. Gholamnia, S. R. Meena, D. Tiede, and J. Aryal. 2019. "Evaluation of Different Machine Learning Methods and Deep-Learning Convolutional Neural Networks for Landslide Detection." *Remote Sensing* 11 (2): 196. <https://doi.org/10.3390/rs11020196>.
- Ghorbanzadeh, O., A. Crivellari, P. Ghamisi, H. Shahabi, and T. Blaschke. 2021. "A Comprehensive Transferability Evaluation of U-Net and ResU-Net for Landslide Detection from Sentinel-2 Data (Case Study Areas from Taiwan, China, and Japan)." *Scientific Reports* 11 (1): 14629. <https://doi.org/10.1038/s41598-021-94190-9>.
- Ghorbanzadeh, O., H. Shahabi, S. T. Pirailou, A. Crivellari, L. E. C. L. Rosa, C. Atzberger, J. Li, et al. 2024. "Contrastive Self-Supervised Learning for Globally Distributed Landslide Detection." *Institute of Electrical and Electronics Engineers Access* 12:118453–118466. <https://doi.org/10.1109/ACCESS.2024.3449447>.
- Ghorbanzadeh, O., Y. Xu, P. Ghamisi, M. Kopp, and D. Kreil. 2022. "Landslide4Sense: Reference Benchmark Data and Deep Learning Models for Landslide Detection." *IEEE Transactions on Geoscience & Remote Sensing* 60:1–17. <https://doi.org/10.1109/TGRS.2022.3215209>.
- Ghorbanzadeh, O., Y. Xu, H. Zhao, J. Wang, Y. Zhong, D. Zhao, Q. Zang, et al. 2022. "The Outcome of the 2022 Landslide4Sense Competition: Advanced Landslide Detection from Multisource Satellite Imagery." *IEEE Journal of Selected Topics in Applied Earth Observations & Remote Sensing* 15:9927–9942. <https://doi.org/10.1109/JSTARS.2022.3220845>.
- Guzzetti, F., S. L. Gariano, S. Peruccacci, M. T. Brunetti, I. Marchesini, M. Rossi, M. Melillo, et al. 2020. "Geographical Landslide Early Warning Systems." *Earth-Science Reviews* 200:102973. <https://doi.org/10.1016/j.earscirev.2019.102973>.
- Guzzetti, F., A. C. Mondini, M. Cardinali, F. Fiorucci, M. Santangelo, and K.-T. Chang. 2012. "Landslide Inventory Maps: New Tools for an Old Problem." *Earth-Science Reviews* 112 (1–2): 42–66. <https://doi.org/10.1016/j.earscirev.2012.02.001>.
- Jelének, J., and V. Kopačková-Strnadová. 2021. "Synergic Use of Sentinel-1 and Sentinel-2 Data for Automatic Detection of Earthquake-Triggered Landscape Changes: A Case Study of the 2016 Kaikoura Earthquake (Mw 7.8)." *New Zealand Remote Sensing of Environment* 265:112634. <https://doi.org/10.1016/j.rse.2021.112634>.
- Jin, Y., X. Liu, and X. Huang. 2024. "EMR-HRNet: A Multi-Scale Feature Fusion Network for Landslide Segmentation from Remote Sensing Images." *Sensors (Switzerland)* 24 (11): 3677. <https://doi.org/10.3390/s24113677>.
- Joshi, N., M. Baumann, A. Ehammer, R. Fensholt, K. Grogan, P. Hostert, M. Jepsen, et al. 2016. "A Review of the Application of Optical and Radar Remote Sensing Data Fusion to Land Use Mapping and Monitoring." *Remote Sensing* 8 (1): 70. <https://doi.org/10.3390/rs8010070>.
- Konishi, T., and Y. Suga. 2019. "Landslide detection with ALOS-2/PALSAR-2 data using convolutional neural networks: A case study of the 2018 Hokkaido Eastern Iburi earthquake."

- In C. Notarnicola, N. Pierdicca, F. Bovenga, and E. Santi, (Eds.), *Active and Passive Microwave Remote Sensing for Environmental Monitoring III* (Vol. 11154, p. 111540H). SPIE. <https://doi.org/10.1117/12.2531695>.
- Lacroix, P., A. L. Handwerger, and G. Bièvre. 2020. "Life and Death of Slow-Moving Landslides." *Nature Reviews Earth and Environment* 1 (8): 404–419. <https://doi.org/10.1038/s43017-020-0072-8>.
- Lei, T., Y. Zhang, Z. Lv, S. Li, S. Liu, and A. K. Nandi. 2019. "Landslide Inventory Mapping from Bitemporal Images Using Deep Convolutional Neural Networks." *IEEE Geoscience Remote Sensing Letter* 16 (6): 982–986. <https://doi.org/10.1109/LGRS.2018.2889307>.
- Li, H., Y. He, Q. Xu, J. Deng, W. Li, and Y. Wei. 2022. "Detection and Segmentation of Loess Landslides via Satellite Images: A Two-Phase Framework." *Landslides* 19 (3): 673–686. <https://doi.org/10.1007/s10346-021-01789-0>.
- Lindsay, E., A. Jarna, G. Ganerød, G. Devoli, J. Reiche, S. Nordal, R. Frauenfelder, et al. 2023. *Understanding landslide expression in SAR backscatter data: A global study*. Preprints.org. <https://doi.org/10.20944/preprints202302.0390.v1>.
- Liu, P., Y. Wei, Q. Wang, Y. Chen, and J. Xie. 2020. "Research on Post-Earthquake Landslide Extraction Algorithm Based on Improved U-Net Model." *Remote Sensing* 12 (5): 894. <https://doi.org/10.3390/rs12050894>.
- Lu, P., W. Shi, Q. Wang, Z. Li, Y. Qin, and X. Fan. 2021. "Co-Seismic Landslide Mapping Using Sentinel-2 10-M Fused NIR Narrow, Red-Edge, and SWIR Bands." *Landslides* 18 (6): 2017–2037. <https://doi.org/10.1007/s10346-021-01636-2>.
- Meena, S. R., L. Nava, K. Bhuyan, S. Puliero, L. P. Soares, H. C. Dias, M. Floris, et al. 2023. "HR-GLDD: A Globally Distributed Dataset Using Generalized Deep Learning (DL) for Rapid Landslide Mapping on High-Resolution (HR) Satellite Imagery." *Earth System Science Data* 15 (7): 3283–3298. <https://doi.org/10.5194/essd-15-3283-2023>.
- Meena, S. R., L. P. Soares, C. H. Grohmann, C. van Westen, K. Bhuyan, R. P. Singh, M. Floris, et al. 2022. "Landslide Detection in the Himalayas Using Machine Learning Algorithms and U-Net." *Landslides* 19 (5): 1209–1229. <https://doi.org/10.1007/s10346-022-01861-3>.
- Microsoft Open Source, M., R. Emanuele, D. Morris, and T. Augspurger. 2022. *Microsoft/planetarycomputer*: October 2022.
- Mondini, A. C., F. Guzzetti, K.-T. Chang, O. Monserrat, T. R. Martha, and A. Manconi. 2021. "Landslide Failures Detection and Mapping Using Synthetic Aperture Radar: Past, Present and Future." *Earth-Science Reviews* 216:103574. <https://doi.org/10.1016/j.earscirev.2021.103574>.
- Nava, L., K. Bhuyan, S. R. Meena, O. Monserrat, and F. Catani. 2022. "Rapid Mapping of Landslides on SAR Data by Attention U-Net." *Remote Sensing* 14 (6): 1449. <https://doi.org/10.3390/rs14061449>.
- Nava, L., O. Monserrat, and F. Catani. 2022. "Improving Landslide Detection on SAR Data Through Deep Learning." *IEEE Geoscience Remote Sensing Letter* 19:1–5. <https://doi.org/10.1109/LGRS.2021.3127073>.
- Orynbaikyzy, A., U. Gessner, and C. Conrad. 2019. "Crop Type Classification Using a Combination of Optical and Radar Remote Sensing Data: A Review." *International Journal of Remote Sensing* 40 (17): 6553–6595. <https://doi.org/10.1080/01431161.2019.1569791>.
- Orynbaikyzy, A., U. Gessner, B. Mack, and C. Conrad. 2020. "Crop Type Classification Using Fusion of Sentinel-1 and Sentinel-2 Data: Assessing the Impact of Feature Selection, Optical Data Availability, and Parcel Sizes on the Accuracies." *Remote Sensing* 12 (17): 2779. <https://doi.org/10.3390/rs12172779>.
- Ozturk, U., E. Bozzolan, E. A. Holcombe, R. Shukla, F. Pianosi, and T. Wagener. 2022. "How Climate Change and Unplanned Urban Sprawl Bring More Landslides." *Nature* 608 (7922): 262–265. <https://doi.org/10.1038/d41586-022-02141-9>.
- Plank, S., A. Tuele, and S. Martinis. 2016. "Landslide Mapping in Vegetated Areas Using Change Detection Based on Optical and Polarimetric SAR Data." *Remote Sensing* 8 (4): 307. <https://doi.org/10.3390/rs8040307>.
- Prakash, N., A. Manconi, and S. Loew. 2020. "Mapping Landslides on EO Data: Performance of Deep Learning Models Vs. Traditional Machine Learning Models." *Remote Sensing* 12 (3): 346. <https://doi.org/10.3390/rs12030346>.
- Prakash, N., A. Manconi, and S. Loew. 2021. "A New Strategy to Map Landslides with a Generalized Convolutional Neural Network." *Scientific Reports* 11 (1): 9722. <https://doi.org/10.1038/s41598-021-89015-8>.
- Roberts, D. R., V. Bahn, S. Ciuti, M. S. Boyce, J. Elith, G. Guillerá-Arroita, S. Hauenstein, et al. 2017. "Cross-Validation Strategies for Data with Temporal, Spatial, Hierarchical, or Phylogenetic Structure." *Holarctic Ecology* 40 (8): 913–929. <https://doi.org/10.1111/ecog.02881>.
- Ronneberger, O., P. Fischer, and T. Brox. 2015. "U-Net: Convolutional Networks for Biomedical Image Segmentation." In: N. Navab, J. Hornegger, W. Wells, A. Frangi (eds). *Medical Image Computing and Computer-Assisted Intervention – MICCAI 2015*. Lecture Notes in Computer Science, vol 9351. Springer, Cham. https://doi.org/10.1007/978-3-319-24574-4_28.
- Sameen, M. I., and B. Pradhan. 2019. "Landslide Detection Using Residual Networks and the Fusion of Spectral and Topographic Information." *Institute of Electrical and Electronics Engineers Access* 7:114363–114373. <https://doi.org/10.1109/ACCESS.2019.2935761>.
- Sivasankar, T., S. Ghosh, and M. Joshi. 2021. "Exploitation of Optical and SAR Amplitude Imagery for Landslide Identification: A Case Study from Sikkim, Northeast India." *Environmental Monitoring and Assessment* 193 (7): 386. <https://doi.org/10.1007/s10661-021-09119-6>.
- Soares, L. P., H. C. Dias, G. P. B. Garcia, and C. H. Grohmann. 2022. "Landslide Segmentation with Deep Learning: Evaluating Model Generalization in Rainfall-Induced Landslides in Brazil." *Remote Sensing* 14 (9): 2237. <https://doi.org/10.3390/rs14092237>.
- Soares, L. P., H. C. Dias, C. H. Grohmann, G. S. Hayakawa, G. H. Rossi, and L. D. P. Soares. 2020. "Landslide Segmentation with U-Net: Evaluating Different Sampling Methods and Patch Sizes." *Revista do Colegio Brasileiro de Cirurgioes* 47. <https://doi.org/10.1590/0100-6991e-20202460>.
- Tehrani, F. S., M. Calvella, Z. Liu, L. Zhang, and S. Lacasse. 2022. "Machine Learning and Landslide Studies: Recent Advances and Applications." *Natural Hazards* 114 (2): 1197–1245. <https://doi.org/10.1007/s11069-022-05423-7>.
- van Westen Cj, van Asch TwjR. Soeters, C. J. van Westen, and T. W. J. van Asch. 2006. "Landslide Hazard and Risk Zonation—Why is it Still so Difficult?" *Bulletin of Engineering Geology*

- and the Environment* 65 (2): 167–184. <https://doi.org/10.1007/s10064-005-0023-0>.
- Wang, H., L. Zhang, K. Yin, H. Luo, and J. Li. 2021. "Landslide Identification Using Machine Learning." *Geoscience Frontiers* 12 (1): 351–364. <https://doi.org/10.1016/j.gsf.2020.02.012>.
- Wang, J., K. Sun, T. Cheng, B. Jiang, C. Deng, Y. Zhao, D. Liu, et al. 2021. "Deep High-Resolution Representation Learning for Visual Recognition." *IEEE Transactions on Pattern Analysis and Machine Intelligence* 43 (10): 3349–3364. <https://doi.org/10.1109/TPAMI.2020.2983686>.
- Wang, Y., H. Gao, S. Liu, D. Yang, A. Liu, and G. Mei. 2025. "Landslide Detection Based on Deep Learning and Remote Sensing Imagery: A Case Study in Linzhi City." *Natural Hazards Research* 5 (1): 95–108. <https://doi.org/10.1016/j.nhres.2024.07.001>.
- Woodard, J. B., B. B. Mirus, M. M. Crawford, D. Or, B. A. Leshchinsky, K. E. Allstadt, N. J. Wood, et al. 2023. "Mapping Landslide Susceptibility Over Large Regions with Limited Data." *JGR Earth Surface* 128 (5): e2022JF006810. <https://doi.org/10.1029/2022JF006810>.
- Xu, Y., C. Ouyang, Q. Xu, D. Wang, B. Zhao, and Y. Luo. 2024. "CAS Landslide Dataset: A Large-Scale and Multisensor Dataset for Deep Learning-Based Landslide Detection." *Scientific Data* 11 (1): 12. <https://doi.org/10.1038/s41597-023-02847-z>.
- Yang, S., Y. Wang, P. Wang, J. Mu, S. Jiao, X. Zhao, Z. Wang, et al. 2022. "Automatic Identification of Landslides Based on Deep Learning." *Applied Sciences* 12 (16): 8153. <https://doi.org/10.3390/app12168153>.
- Yang, Z., and C. Xu. 2022. "Efficient Detection of Earthquake-triggered Landslides Based on U-Net++: An Example of the 2018 Hokkaido Eastern Iburi (Japan) Mw = 6.6 Earthquake." *Remote Sensing* 14 (12): 2826. <https://doi.org/10.3390/rs14122826>.
- Yi, Y., and W. Zhang. 2020. "A New Deep-Learning-Based Approach for Earthquake-Triggered Landslide Detection from Single-Temporal RapidEye Satellite Imagery." *IEEE Journal of Selected Topics in Applied Earth Observations and Remote Sensing* 13:6166–6176. <https://doi.org/10.1109/JSTARS.2020.3028855>.
- Zhang, T., W. Zhang, D. Cao, Y. Yi, and X. Wu. 2022. "A New Deep Learning Neural Network Model for the Identification of InSAR Anomalous Deformation Areas." *Remote Sensing* 14 (11): 2690. <https://doi.org/10.3390/rs14112690>.
- Zhong, C., Y. Liu, P. Gao, W. Chen, H. Li, Y. Hou, T. Nuremanguli, et al. 2020. "Landslide Mapping with Remote Sensing: Challenges and Opportunities." *International Journal of Remote Sensing* 41 (4): 1555–1581. <https://doi.org/10.1080/01431161.2019.1672904>.